Encapsulated crystallisation inhibitor as a long-term solution to mitigate salt damage in hydraulic mortars

Kamat, Ameya; Schlangen, Erik; Lubelli, Barbara

DOI
10.1016/j.cemconcomp.2024.105682

Publication date
2024

Document Version
Final published version

Published in
Cement and Concrete Composites

Citation (APA)
Kamat, A., Schlangen, E., & Lubelli, B. (2024). Encapsulated crystallisation inhibitor as a long-term solution to mitigate salt damage in hydraulic mortars. *Cement and Concrete Composites*, *152*, Article 105682. https://doi.org/10.1016/j.cemconcomp.2024.105682

Cement and Concrete Composites 152 (2024) 105682

Contents lists available at ScienceDirect

Cement and Concrete Composites

journal homepage: www.elsevier.com/locate/cemconcomp

Encapsulated crystallisation inhibitor as a long-term solution to mitigate salt damage in hydraulic mortars

Ameya Kamat [a,b,*], Erik Schlangen [b], Barbara Lubelli [a]

[a] Heritage and Architecture, Architecture and Built Environment, Delft University of Technology, the Netherlands
[b] Materials and Environment, Civil Engineering and Geosciences, Delft University of Technology, the Netherlands

ARTICLE INFO

Keywords:
Sodium ferrocyanide
Chitosan-calcium alginate
Leaching
Salt damage
Accelerated weathering
Plasters

ABSTRACT

Salt (NaCl) weathering in mortar, can be mitigated by incorporating a crystallisation inhibitor (sodium ferrocyanide) during mortar preparation. However, the service-life of the inhibitor is limited, due to its susceptibility to leaching out of mortar. Encapsulating the inhibitor in chitosan-calcium alginate capsules has demonstrated controlled-release of the inhibitor and therefore, reduction in its leaching. Nevertheless, the addition of capsules may have a negative effect on mortar's properties and/or its salt-weathering resistance. In this research, natural hydraulic lime (NHL) and commercial cement-based mortars were prepared, with encapsulated inhibitor and with directly mixed-in inhibitor. Mechanical and physical properties of mortars were assessed experimentally. An accelerated NaCl-weathering test was performed to assess the durability of mortar to salt damage. The damage evolution was assessed visually and by quantifying material loss, efflorescence and leaching of the inhibitor. At the end of the test, crystal morphology inside the pores was examined using SEM. The results show that adding inhibitor, both in encapsulated and mixed-in form, had a negligible effect on the properties of NHL and cement-based mortars. Compared to the reference mortar without inhibitor, NHL-mortars with mixed-in inhibitor and encapsulated inhibitor had a better durability to salt damage, showing negligible material loss. The capsules facilitated controlled-release and reduced leaching of the inhibitor. In cement-based mortars including the reference, no damage was observed; still, the inhibitor was shown to be effective in modifying the salt crystal habit. The results show that encapsulation of the inhibitor can improve the service-life of the mortar without compromising its performance.

1. Introduction

Salt weathering is responsible for severe damage in porous building materials [1]. Commonly occurring soluble salts, such as sodium chloride (NaCl), permeate in building materials from various sources such as ground water, salt spray and de-icing salts [2] and, due to evaporation or temperature changes, crystallise within the pores. Crystallisation of salts under supersaturated conditions can exert crystallisation pressure on the pore walls [3] causing damage when the pressure exceeds materials' mechanical strength [4]. In particular for NaCl, repeated exposure to crystallisation-deliquescence cycles has shown to increase the crystal volume [5] and consequently accelerate the damage propagation [6]. Plasters and renders, also because of their location at the surface of the buildings, are exposed to repeated crystallisation-deliquescence cycles, due to evaporation and exposure to changing climatic conditions. Therefore, plasters and renders need frequent replacements, and entail high maintenance costs. Improving the durability of plasters and renders with respect to salt damage can reduce their replacement frequency and minimise costs. Incorporation of crystallisation inhibitors in mortars has shown encouraging results in improving the durability of plasters/-renders by preventing and/or delaying salt damage [7].

Crystallisation inhibitors are chemical additives that inhibit crystal nucleation and growth by adsorbing preferentially on specific crystal faces [8]. Crystallisation inhibitors are selective to specific salts. As an example, phosphonate based inhibitors that have shown to be effective against sodium sulphate (Na_2SO_4) crystallisation [9], do not have any effect on the crystallisation of NaCl [10]. For NaCl, several inhibitors exist, such as alkali ferrocyanides, cadmium chloride, sodium metaphosphate and iron (III) meso-tartaric acid [11,12]. However, compared to alkali ferrocyanides, these inhibitors require a high concentration to inhibit NaCl crystallisation and are effective only in a limited pH range [13]. Sodium ferrocyanide ($Na_4Fe(CN)_6$, hereafter referred as NaFeCN)

* Corresponding author. Delft University of Technology, Faculty of Architecture, Julianalaan 134, 2628BL, Delft, the Netherlands.
E-mail address: a.a.kamat@tudelft.nl (A. Kamat).

https://doi.org/10.1016/j.cemconcomp.2024.105682
Received 15 April 2024; Received in revised form 16 July 2024; Accepted 23 July 2024
Available online 24 July 2024

is one of the most effective crystallisation inhibitors of alkali halides, and in particular of NaCl [14]. Hexacyanoferrate ions [$Fe(CN_6)^{4-}$] from NaFeCN preferentially sorb on the {100} faces of the NaCl crystals, and block further crystal growth due to a charge mismatch [12]. As a consequence, the rate of crystal growth is suppressed along ⟨100⟩and the crystal morphology changes from a cubic crystal to a dendritic (skeletal) habit [15,16]. When introduced to NaCl contaminated porous building materials, NaFeCN has shown to favour crystallisation of harmless efflorescence (surface crystallisation) over harmful subflorescence (confined in-pore crystallisation) and in doing so, has greatly reduced the associated salt damage [16–19]. The reduced damage has been attributed to a delay in NaCl nucleation and crystal growth due to NaFeCN, providing longer time for salt ions to be transported to the evaporation surface [16]. Moreover, the formation of dendritic crystals with a higher surface area has shown to increase the evaporation rate and promote advection of salt ions towards the surface [20]. Recently, a new hypothesis to explain reduced salt damage has been proposed based on the smaller NaCl crystal size observed in presence of NaFeCN. Smaller NaCl crystals, by occupying smaller volume can prevent pore clogging and decrease crystallisation pressure [7]. Incorporating NaFeCN during the production of hydrated lime mortars has been highly effective in reducing salt damage in the laboratory [7,21,22] as well as in the field [23]. Early studies show that addition of inhibitor does not affect the properties of hydraulic mortars [24], making the inhibitor also suitable for hydraulic mortar applications. However, the effect of the combination of inhibitor in hydraulic mortars with respect to salt damage is not yet investigated.

Despite the positive results reported on lime-based mortars with mixed-in inhibitors, a high depletion of NaFeCN from mortar specimens after successive wetting-drying cycles was observed and attributed to the leaching of NaFeCN [7]. A study specifically focused on the leaching behaviour of NaFeCN from mortar specimens reported severe leaching, and concluded that directly adding NaFeCN to mortar may not prevent salt damage over a long time period [25]. In a recent pilot study, we demonstrated that introducing NaFeCN in chitosan-calcium alginate (CsCA) capsules lead to a controlled release and reduced leaching of the inhibitor from mortar specimens [26]. The controlled-release of the inhibitor from the capsules was attributed to two factors (i) the role of chitosan in CsCA capsules to counteract the swelling of alginate matrices, and thereby reduce capsule permeability in response to pH changes [26,27] and (ii) electrostatic attraction of positively charged chitosan to negatively charged [$Fe(CN_6)^{4-}$] that slowed down the outward diffusion of the inhibitor [26]. Additionally, it was found that chitosan to alginate ratio of 0.25 lead to the most optimal solution and was effective in delaying the transport and significantly reducing the diffusion coefficient of the leached inhibitor in mortar [26]. To develop this technology further, some issues pertaining to the introduction of encapsulated NaFeCN in mortar need to be clarified. A first issue concerns the impact of CsCA capsules on the mortar properties, such as mechanical strength and workability, as past research has shown negative impact of capsules and capsule-like materials on the properties of concrete [28,29]. Another issue concerns if mortars with encapsulated inhibitor offer similar resistance against salt damage as mortars with mixed-in inhibitor, while slowing down the inhibitor leaching.

To resolve the above issues, two different types of hydraulic mortars-Natural hydraulic lime and commercial two-layer cement-based plasters containing encapsulated inhibitor as well as mixed-in inhibitor are tested. The research is divided in two parts. In the first part, the effect of capsules on the properties of mortars is investigated (Section 2.4). In the second part, the salt weathering resistance of mortars and the leaching of inhibitor is assessed (Section 2.5).

2. Materials and methods

2.1. Materials

For the preparation of capsules (Section 2.2), lab grade sodium alginate (mannuronic/guluronic ratio of 1.56), chitosan (Molecular weight: 190–310 kDa), calcium chloride ($CaCl_2{\cdot}2H_2O$) were obtained from Sigma Aldrich. Acetic acid (CH_3COOH) was obtained from J.T. Baker and sodium ferrocyanide decahydrate ($Na_4Fe(CN)_6{\cdot}10H_2O$) used as the crystallisation inhibitor was obtained from Acros organics.

In the preparation of mortar specimens (Section 2.3), Natural hydraulic lime (binder, St. Astier) with a strength class of 3.5 MPa, SP-Levell® (ready-mix mortar, Remmers), SP-Top SR® (ready-mix mortar, Remmers) and standard river sand (0.08–2 mm) as per [30] were used. Maastricht limestone (Netherlands) with a porosity of 50 % v/v and a mean pore size of 30 μm [31] was used as a substrate.

2.2. Preparation of chitosan-calcium alginate capsules containing NaFeCN

The capsules containing sodium ferrocyanide (NaFeCN) were prepared and characterised according to a procedure that is elaborated in

Table 1
Description of test specimens and explanation of the labels.

Binder	Specimen label	Description	Geometry	Size
NHL	NHL-R	NHL reference specimens i.e. without NaFeCN and capsules	Prisms	160x40x40 mm
			Discs	Ø = 50 mm, H = 20 mm
			Stone-mortar cylinder	Ø = 50 mm, H = 50 mm (including stone)
	NHL-F	NHL specimens with mixed-in NaFeCN	Prisms	160x40x40 mm
			Discs	Ø = 50 mm, H = 20 mm
			Stone-mortar cylinder	Ø = 50 mm, H = 50 mm (including stone)
	NHL-CsCA-F	NHL specimens containing CsCA-F capsules	Prisms	160x40x40 mm
			Discs	Ø = 50 mm, H = 20 mm
			Stone-mortar cylinder	Ø = 50 mm, H = 50 mm (including substrate)
2-layer plaster: SP-Levell®(bottom layer) + SP-Top® (top layer)	2L-R	2-layer plaster reference specimens	stone-mortar cylinder	Ø = 50 mm, H = 50 mm (including substrate)
	2L-CsCA-F	2-layer plaster with CsCA-F capsules in the bottom layer	stone-mortar cylinder	Ø = 50 mm, H = 50 mm (including stone)
SP-Levell®	SPL	SP-Levell reference specimens	Prisms	160x40x40 mm
			Discs	Ø = 50 mm, H = 20 mm
	SPL-CsCA-F	SP-Levell specimens With CsCA-F capsules	Prisms	160x40x40 mm
			Discs	Ø = 50 mm, H = 20 mm
SP-Top®	SPT	SP-Top reference specimens	Prisms	160x40x40 mm
			Discs	Ø = 50 mm, H = 20 mm

Table 2
An overview of the characterisation tests performed on different mortar specimens.

Material property	Method	Standard	Type of mortar	Specimen type	Replicates
Workability	Flow table test	NEN-EN-1015-3	NHL-R, NHL-F, NHL-CsCA-F, SPL, SPL-CsCA, SPT	Fresh state	2
Compressive strength	Mechanical testing	NEN-EN-1015-11		Prism	3
Pore size distribution Open porosity Bulk density	MIP	–		Disc (1 cm^3 sample)	2
Water absorption coefficient	Capillary absorption/ gravimetric	NEN-EN-1925		Disc	3
Drying rate	Gravimetry	–		Disc	3
Microscopic examination	PFM	–	NHL-CsCA-F	Disc (thin-section)	1
	SEM	–	NHL-CsCA-F	Disc, (polished section)	1

our past research as a two-step process [26,27]. In the first step, calcium alginate containing NaFeCN capsules were prepared using ionic gelation [32]. The procedure of ionic gelation was chosen as the procedure could be carried out using a simple low-cost technique, such as extrusion dripping. In ionic gelation, the alginate mixture containing desired cargo crosslinks ionically with divalent Ca^{2+} ions on contact, to form robust 3D hydrogel capsules encapsulating the cargo [33]. Herein, a mixture of sodium alginate (2 % w/v) and NaFeCN (4 % w/v) was extruded drop by drop in a cross-linking bath containing a mixture of calcium chloride (3 % w/v) and NaFeCN (4 % w/v) using a peristaltic pump (Masterflex console drive, Cole Parmer instruments) to form calcium alginate capsules with encapsulated NaFeCN. The capsules were washed using demineralised water to remove unlinked Ca^{2+} ions. In the second step, the obtained capsules were added to a bath of 0.5 % w/v chitosan (Cs) in 0.1 M acetic acid and stirred at 300 rpm for 15 min to form a polyelectrolyte complex of chitosan-calcium alginate capsules containing NaFeCN (CsCA-F). The CsCA-F capsules were dried in an oven at 40 ± 2 °C for 48 h and stored in air-tight containers.

When dry, the CsCA-F capsules had an ellipsoidal form with a maximum diameter of 1063 ± 124 μm, a minimum diameter of 730 ± 85.5 μm. The average encapsulated amount of NaFeCN was 264 mg g^{-1} of dry capsule mass [26].

2.3. Preparation of test specimens

2.3.1. NHL-based mortar specimens

Different types of natural hydraulic lime (NHL) mortar specimens were prepared (see Table 1) (i) Reference mortar specimens without NaFeCN and capsules (**NHL-R**) were prepared by mixing NHL with river sand in a 1:3 ratio by volume and a water to binder ratio (w/b) of 1.17 to achieve a 165 mm flow as per NEN-EN-459-2 [34]. (ii) mortar specimens with mixed-in NaFeCN (**NHL-F)** prepared in the same way as NHL-R, but with addition of NaFeCN at a concentration of 1 % weight of the binder. NaFeCN was first dissolved in water to be used for mortar preparation, and then added to NHL and sand. (iii) mortar specimens containing NaFeCN encapsulated in CsCA-F capsules (**NHL-CsCA-F**) were prepared in the same way as NHL-R, but with addition of CsCA-F capsules. The amount of capsule was defined such that the total NaFeCN content was 1 % weight of the binder; this resulted in an amount of capsules equal to 3.78 % of the binder weight.

The type of specimens/geometry differed based on characterisation and weathering tests (see Table 1). Mortar specimens to be used for mechanical testing were cast as prims (160x40x40) mm as per NEN-EN-1015-11 [35].

Stone-mortar combination specimens to be used for the salt weathering test were casted in the following way. Freshly mixed mortar was cast on pre-wetted, cylindrical (Ø = 50 mm, H = 30 mm) Maastricht limestone substrate in polyvinyl chloride (PVC) moulds. The mortar thickness was 20 mm, and the total size of the stone-mortar specimen was Ø = 50 mm and H = 50 mm. The mortar was compacted by hand, using a trowel.

Mortar specimens to be used in the physical characterisation tests were prepared on Maastricht limestone substrate, in the same way as those for the salt weathering test, and then detached after 4 days. A paper towel was placed in between the substrate and the mortar during casting, to allow for easy detachment of the mortar to obtain mortar discs (Ø = 50 mm, H = 20 mm).

All specimens were covered with a plastic film and cured for one week at 20±2 °C, 95 ± 5 % relative humidity (RH); subsequently, they were demoulded and cured at lab conditions (20 ± 3 °C, 55 ± 5 °C) for at least three weeks as per NEN-EN-1015-11 before testing [34].

2.3.2. Two-layer plaster (cement-based)

A two-layer cement-based plaster system, commercially available and commonly used in renovation for application on salt loaded substrate was selected. The system is composed of a bottom (base) layer mortar (SP-Levell, Remmers) and a top layer mortar (SP-top SR, Remmers); the top layer is hydrophobic and is meant to stop salt transport to the surface, leading to accumulation of the salts in the inner layer.

Characterisation tests were performed on individual cement mortars while the salt weathering test was performed on the composite two-layer plaster system. Different types of specimens were prepared for this study and an overview is presented in Table 1.

For different characterisation tests (Table 2), Cement-based mortar components of the two-layer plaster system were cast separately and labelled as (i) SP-Top (**SPT**) (ii) SP-Levell (**SPL**) and (iii) SP-Levell containing CsCA-F capsules (**SPL-CsCA-F**). The amount of mixing water was based on the manufacturer's specifications i.e. 325 mL kg^{-1} for SP-Levell and 250 mL kg^{-1} for SP-Top. The amount of capsules in SPL-CsCA-F specimens was 0.45 % of the dry weight of SP-Levell. Specimens to be used for mechanical testing were cast as prims (160x40x40) mm as per NEN-EN-1015-11 [35]. Specimens used for physical characterisation test (Table 2) were cast as discs (Ø = 50 mm, H = 20 mm) in the same way as NHL specimens (Section 2.3.1).

For salt weathering test, stone-mortar specimens were prepared in the same was as NHL-based mortar specimens (Section 2.3.1) where Maastricht limestone was used as the substrate and the mortar made of the two-layer plaster system was cast on top of the substrate. Different types of specimens were prepared as follows (i) Reference two layer plaster without NaFeCN and capsules **(2L-R)** where the bottom layer of the plaster (10 mm thick) was prepared by mixing SP-Levell with water. The top layer of the plaster (10 mm thick) was prepared by mixing SP-Top SR with water and cast on top of the bottom layer after 24 h. (ii) **2L-CsCA-F** (Two-layer plaster containing capsules containing NaFeCN) where the bottom layer of the plaster (10 mm thick) was prepared by mixing SP-Levell, and CsCA-F capsules equal to 0.45 % by the weight of SP-Levell (binder + sand). The top layer of the plaster (10 mm thick) was prepared by mixing SP-Top SR and water and cast on top of the bottom layer after 24 h. The capsules were not added to the top layer.

All the specimens were demoulded after 4 days and cured at 20 ±2 °C, 95 ± 5 % RH for 28 days before testing.

2.4. Characterisation of mortar specimens

The effect of capsules on the fresh and hardened properties of mortar (Table 1) was assessed using various experimental techniques (Table 2). The workability of freshly mixed mortar was assessed as per NEN-EN-1015-3 [36] using the flow table test. The compressive strength was measured on the mortar prisms after 28 days of curing, per NEN-EN-1015-11 [35] with a loading rate of 0.1 kN s^{-1}.

The open porosity, bulk density and pore size distribution of all mortars were measured using mercury intrusion porosimetry (MIP, Micromeritics Autopore IV) on samples of approximately 4 g, collected from the mortar discs. Samples were freeze-dried, before starting the measurements and subjected to a maximum intrusion pressure of 210 MPa.

The water absorption coefficient (WAC) was measured on mortar discs (Table 1) as per NEN-EN-1925 [37] through capillary absorption. Mortar discs were dried at 40 °C to a constant weight and their sides sealed with parafilm® (Bemis Company Inc.). The specimens were placed with the bottom surface in water and weighed at prescribed time intervals [37]. The water WAC was calculated as per Eq. (1).

$$WAC = \frac{m_i - m_0}{A.(\sqrt{t_i})} \quad \text{Eq. (1)}$$

Where m_i [g] is the mass of specimen at time interval t_i [s], where the transition takes place between the first absorption stage and the second absorption stage. m_0 [g] is the dry mass of the specimen and A [m^2] is the surface area of the specimen subjected to capillary absorption.

Following capillary absorption, the specimens were subjected to drying at lab conditions (i.e. 23.1 ± 1.1 °C, RH 51.5 ± 5.1 %) and the weight of the specimens was recorded at regular intervals to obtain a drying curve.

In the case of NHL-CsCA-F mortar, one thin-section was prepared to examine the capsule distribution and the mortar porosity. To prepare the thin section, the specimen was first impregnated with an epoxy resin containing a UV-fluorescent dye. The thin-section was prepared following a protocol by Ref. [38]. The images were acquired under plane polarised light and UV-light using Keyence VHX-7000 digital microscope.

One polished cross section was prepared to examine the capsule-mortar interface. The polished section was prepared on an epoxy impregnated specimen that was grinded and polished on a lapping table [31]. The images were obtained under back scattered electron (BSE) setting using a scanning electron microscope (FEI Quanta 650 FEG) at an accelerating voltage of 15 kV.

2.5. Procedure for accelerated salt weathering test

The accelerated salt weathering test is based on the RILEM 271-ASC recommendations [39,40], and further adapted to allow for testing of stone-mortar combination. As for the RILEM 271-ASC, the procedure used in this research consists of two stages (i) contamination and accumulation with salt and (ii) damage propagation.

2.5.1. Contamination and accumulation

The specimens (stone-mortar cylinders, see Table 1) were dried in an oven at 40 °C to a constant weight and the sides were sealed with parafilm and a textile tape. The specimens were then contaminated from the bottom surface via capillary absorption with 10 % w/w NaCl solution; the amount of solution was equivalent to the capillary moisture content of the Maastricht Limestone (31.1 % of the dry weight of the stone). After complete absorption of the solution, the bottom of the specimens were sealed with parafilm and the textile tape, and the specimens were placed in a climate chamber at 40 ± 2 °C and 15 ± 5 % RH until 80 % of the water had evaporated marking the end of the accumulation stage. The specimens were stored in a box inside a climate chamber with a lid made of Japanese paper in order to limit the effect of convection from the ventilator.

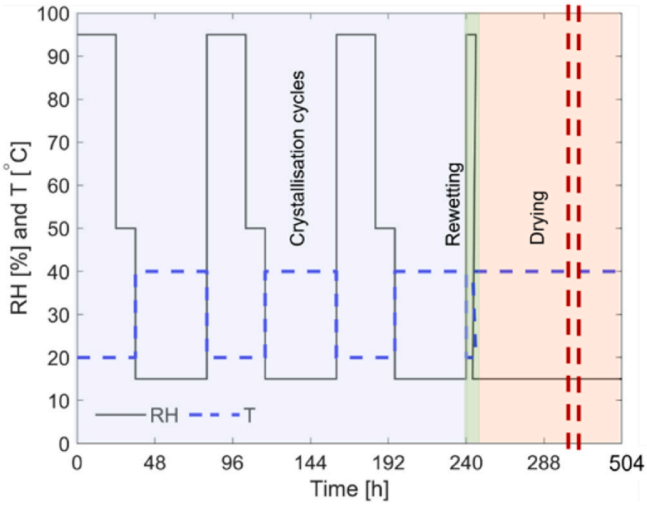

Fig. 1. Relative humidity (RH) and temperature (T) defined for every three-week propagation cycle as per RILEM 271-ASC [39]. First 240h (light blue area) consists of RH and T cycling, followed by 6h rewetting (light green area) and 258h of drying (light orange area). In total, specimens were subjected to four such cycles.

2.5.2. Damage propagation

After the accumulation stage, specimens were subjected to four 3-week cycles of damage propagation. Each 3-week cycle consisted of temperature and RH cycles, as schematised in Fig. 1. In between each 3 week-cycle the specimens were rewetted with an amount of demineralised water equivalent to 30 % by weight of the solution used for initial contamination. The test was carried out in a programmable climatic cabinet (ClimeEvent, Weiss-Technik). Three replicates were used for each type of specimen.

2.5.3. Assessment of damage

Changes to the evaporation surface (top specimen of the mortar) were recorded with a digital camera at the start of the accelerated test, at the end of the accumulation stage and at the end of each 3-week cycle of the propagation stage.

At the end of the test, the material loss, efflorescence and the amount of leached inhibitor from each specimen was measured in the following way. The top surface was brushed with a soft-bristled toothbrush and the collected debris (salt efflorescence plus material loss) was dried to a constant weight at 40 °C and its mass was recorded (m_1). Demineralised water with a mass at least 10 times of the debris weight or 5g which ever was higher was added to the dry debris and the mixture was stirred to dissolve any salts present in the debris. The volume of the added water was recorded as V [L]. After 24 h, the mixture was passed through a medium-speed filtration paper to separate material loss (filter paper) and soluble salts (filtrate). The mass of the material loss after separating the salt efflorescence on the filter paper was recorded (m_2) and the amount of salt efflorescence was calculated as $m_1^- m_2$.

The concentration of Fe(II/III) ions (C_{Fe}) [mg L^{-1}] in the solution was measured by analysing the filtrate using Inductively coupled plasma-optical emission spectroscopy (ICP-OES, PerkinElmer Optima 5300DV). The amount of NaFeCN in the debris was calculated from the ICP-OES measurements using Eq. (2).

$$Leached_{NaFeCN} = C_{Fe} * V * \left(\frac{Mw_{NaFeCN}}{Aw_{Fe}}\right) \quad \text{Eq. (2)}$$

Where, Mw_{NaFeCN} is the molecular weight of NaFeCN (484.06 g mol^{-1})

Table 3
Overview of measured properties in NHL-based mortars and cement-based mortars. The mean values and one standard deviation away from the mean is reported.

Measured property	Test method	NHL-based mortars			Cement-based mortars		
		NHL-R	NHL-F	NHL-CsCA-F	SPT	SPL	SPL-CsCA-F
Workability [mm]	Flow table	166 ± 1	172 ± 3	164 ± 1	154 ± 1	144 ± 1	146 ± 0
Compressive strength [MPa]	Mechanical testing	0.42 ± 0.08	0.39 ± 0.07	0.62 ± 0.08	–	1.82 ± 0.14	1.44 ± 0.16
Porosity [%]	MIP	21.83 ± 0.36	22.35 ± 0.27	22.37 ± 0.06	58.99 ± 0.01	58.54 ± 0.48	55.69 ± 0.43
Bulk density [g mL^{-1}]	MIP	2.03 ± 0.01	2.00 ± 0.00	1.99 ± 0.02	0.93 ± 0.03	0.97 ± 0.02	1.01 ± 0.01
Water absorption coefficient [g $m^{-2}s^{-0.5}$]	Capillary absorption	159.56	147.91	156.64	2.33	26.33	25.36

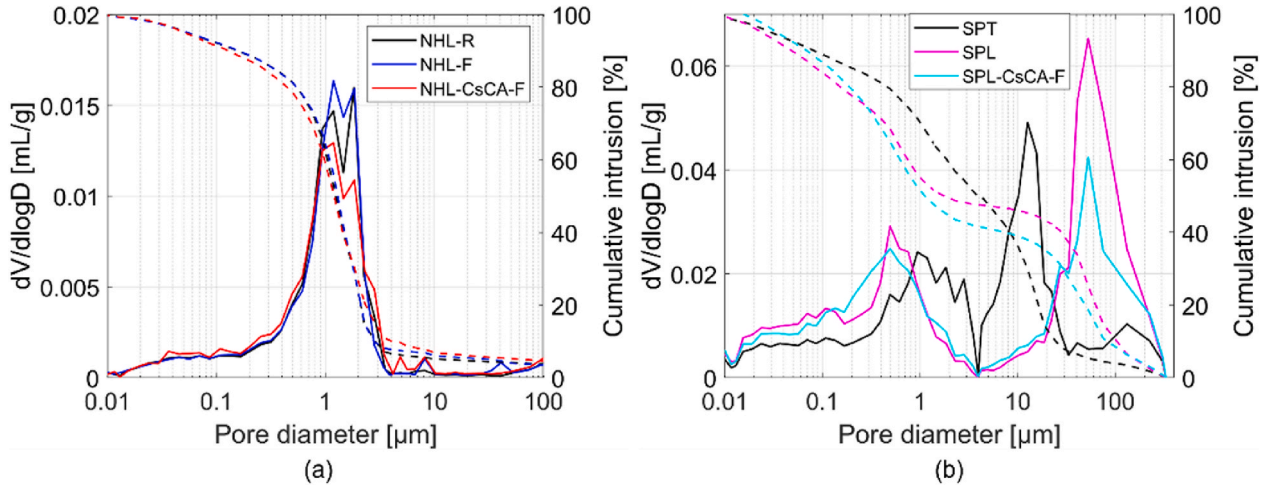

Fig. 2. The pore size distribution measured using mercury intrusion porosimetry. **(a)** NHL-based mortars **(b)** Commercial cement-based mortars.

and Aw_{Fe} is the atomic weight of Fe (55.85 g mol^{-1}). The number of moles of Fe atoms and NaFeCN molecules are equal. The total amount of NaFeCN leached out in the debris [mg] was reported as the percentage of the initial NaFeCN present in the specimen at the start of the test.

SEM (FEI quanta 650 FEG) was performed on the cross-section of one specimen of each mortar type subjected to the accelerated weathering test to examine the salt crystal morphology. The cross-section was obtained by splitting the mortar specimen vertically using a tensile splitting test. The imaging was acquired just below the evaporation surface.

3. Results and discussion

3.1. Effect of the encapsulated inhibitor on the properties of mortar

In NHL-based mortars, the measured workability (flow) of fresh NHL-CsCA-F is similar to NHL-R specimens (Table 3). NHL-F specimens show a slightly higher flow compared to NHL-R with a higher scatter and can be a result of variation in parameters such as mixing speed and mixing time. In cement-based mortars, SPL-CsCA-F specimens show similar workability as the reference mortar SPL (Table 3). The above results show that addition of capsules have a negligible effect on workability of both NHL-based and cement-based mortars. Past studies have shown that hydrophilic polymers such as chitosan or alginate can absorb high volume of mixing water and reduce workability [29]. However, in this study, a reduction in workability was not observed and could be due to a relatively low dose of capsules (3.78 % of the binder weight) used during mortar preparation.

The 28-days compressive strength measured on NHL-CsCA-F specimens is higher than NHL-R and NHL-F (Table 3), showing that addition of capsules do not negatively affect the mechanical properties of NHL-

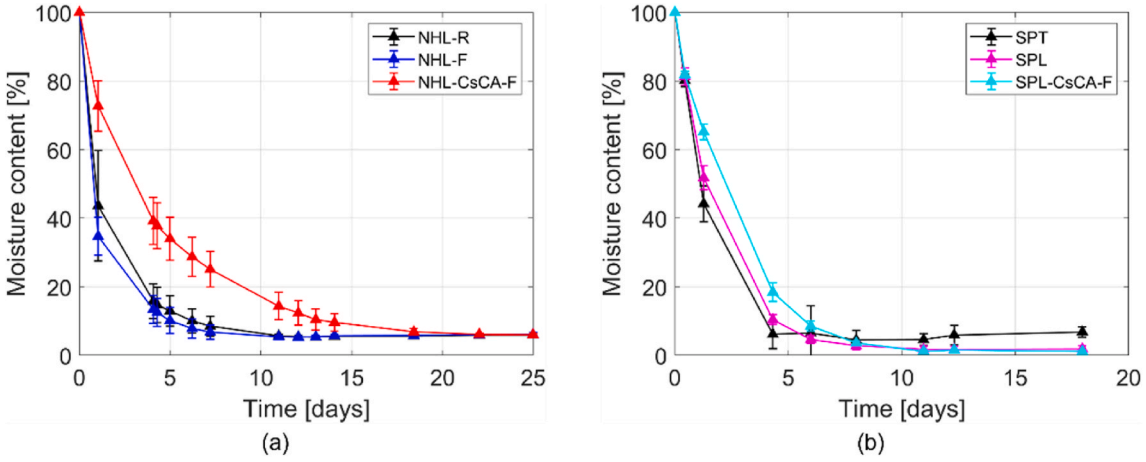

Fig. 3. Drying behaviour of mortars **(a)** NHL-based mortars **(b)** commercial cement-based mortars.

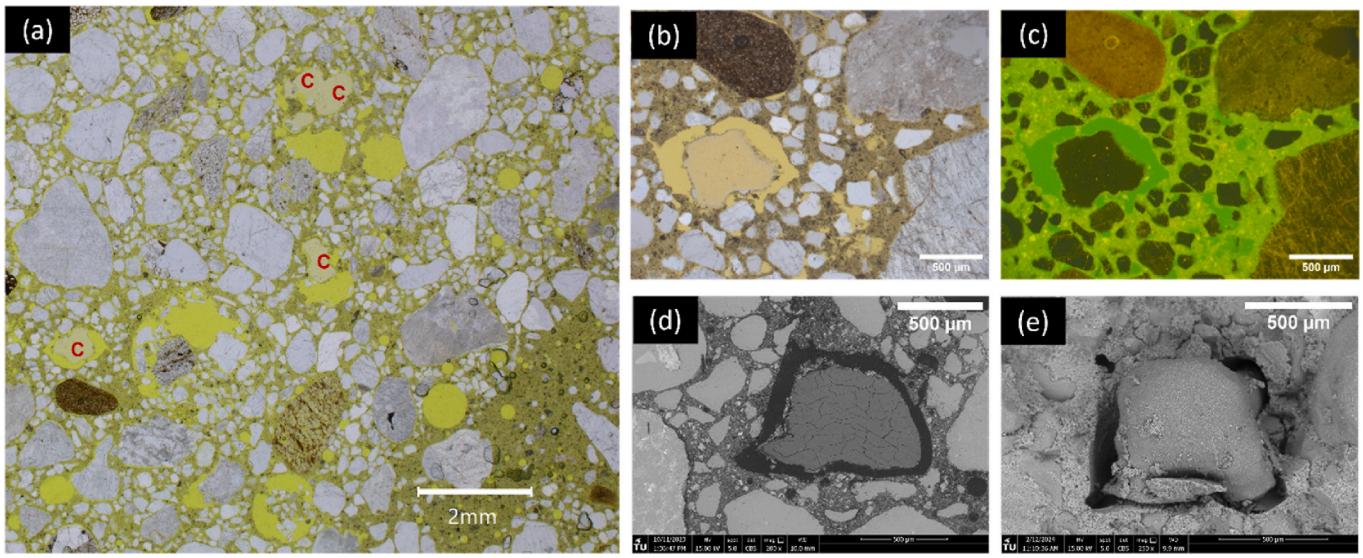

Fig. 4. Microscopy images of CsCA-F capsules in NHL specimens **(a):** Low magnification optical micrograph of a thin-section under plane polarised light (PPL) showing pale yellow capsules (marked in red) distributed in the mortar matrix. **(b)** PPL image showing close up of a capsule. **(c)** UV-light image of the same capsule as (b). The green fluorescence indicates the locations of epoxy impregnation. The image shows epoxy is unable to impregnate in the capsule pores. **(d)** Scanning electron microscope (SEM) image on a polished section showing that the capsules have shrunk during drying, leading to the formation of air-pockets around them. Note the capsules do not form a bond with the mortar matrix. **(e)** SEM-morphology image of a capsule on an unpolished section showing that the capsule remains intact in the hardened mortar and does not bond to the matrix.

based mortars. The 28-day compressive strength of NHL-F and NHL-R is also similar showing that addition of inhibitor also has no effect on the compressive strength and is in agreement with a previous study [24]. Conversely, in cement-based mortars, SPL-CsCA-F specimens have a slightly lower compressive strength as compared to SPL showing that addition of capsules has a minor effect on the compressive strength of cement-based mortars.

When considering the physical properties, all types of NHL-based mortar specimens show similar porosity, and unimodal pore size distribution (Fig. 2a) with a mean pore diameter ranging between 0.5 and 2 µm. Therefore, it can be concluded that the addition of capsules (NHL-CsCA-F) or mixed-in inhibitor (NHL-F) has a negligible effect on the porosity (Table 3) and the pore-size distribution (Fig. 2a).

The cement-based mortars exhibit a bi-modal pore-size distribution (Fig. 2b) with the majority of pore diameters in the range of 10–100 µm and 0.1–2 µm. SPT specimens containing the hydrophobic additive has a similar open porosity but a narrower pores-size distribution than SPL specimens. Different pore-size distribution between SPT and SPL is a result of different mortar composition and water content. To assess the effect of capsules, SPL-CsCA-F and SPL specimens are compared. The porosity measurement is slightly lower in SPL-CsCA-F specimens than SPL specimens (Table 3). The reduction in porosity is evident in the range between 10 and 200 µm (Fig. 2b). It can be concluded that the effect of capsules on the porosity and pore-size distribution of cement-based mortars is minor.

The water absorption coefficient (WAC) of NHL-based mortars is higher than cement-based mortars (Table 3). In NHL-based mortars, the WAC of NHL-CsCA-F and NHL-R is similar. Likewise, In cement-based mortars WAC of SPL-CsCA-F is comparable to its reference (SPL). Presence of capsules, do not have any effect on the capillary absorption as substantiated also by their negligible impact on the pore-size distribution (Fig. 2). Among cement-based mortars, SPT mortar has 10 times lower WAC than SPL. This is expected and is due to the hydrophobic character of this mortar.

The drying behaviour of both NHL-based and cement-based mortars (Fig. 3) show that the specimens containing capsules dry slower. The drying rate is significantly slower in NHL-CsCA-F specimens as compared to both NHL-R and NHL-F specimens (Fig. 3a). Similarly, in cement-based mortars, SPL-CsCA-F specimens show a slower drying rate than the reference SPL specimens (Fig. 3b); this difference, however, is less prominent as compared to NHL-based mortars. These results clearly show that the slow drying is a consequence of the capsule addition and not NaFeCN.

The slow drying rate observed in presence of CsCA-F capsules may be attributed to the hydrophilic nature [41,42] of chitosan and alginate making them hygroscopic. Slow drying can even be beneficial to prolong mortar hydration and reduce shrinkage, by providing a steady supply of moisture and facilitating internal curing, in a similar manner as super-absorbent polymers [43]. The higher compressive strength in NHL-based mortar specimens containing the capsules (Table 3) can be explained by the extended hydration provided due to slower drying. NHL mortars were cured for three weeks at laboratory conditions (20 ± 3 °C, 55 ± 5 °C), meaning that the low degree of hydration in the NHL-R specimens due to faster evaporation of moisture is probably improved in NHL-CsCA-F due to slower loss of moisture. However, an increase in compressive strength is not observed in cement-based mortars (Table 3). SPL and SPL-CsCA-F mortars were cured at a high relative humidity (20 ± 2 °C, 95 ± 5 °C), where possibly the hydration is not hindered. In this situation, the internal curing provided by the capsules is not evident/relevant. In fact, a slightly lower compressive strength as measured on SPL-CsCA-F specimens can be a result of the introduction of air pockets and weak interfacial transition zones (ITZ) between the capsules and the mortar matrix [44] as evident in Fig. 4b–e.

Microscopic examination of the capsules in hardened mortar is presented in Fig. 4. This shows that the capsules are well distributed in the mortar mix (Fig. 4a) and are able to survive the mixing process (Fig. 4a–e). The capsules have a pale yellow appearance; around the capsules an air-pocket is visible (Fig. 4b and c). The formation of air pockets shows that the capsules shrink as they lose moisture. It is possible to observe that the epoxy resin (green fluorescence due to UV excitation) (Fig. 4c) which easily penetrates in the mortar matrix, but does not penetrate in the dry capsules; this suggests that the pores of the capsule must be smaller than those of the mortar matrix. The diffusive release of NaFeCN from CsCA capsules is dependent on the pore size of the capsules [26]. Smaller pores of the capsules relative to mortar matrix show that the capsules have a better chance of retaining NaFeCN than

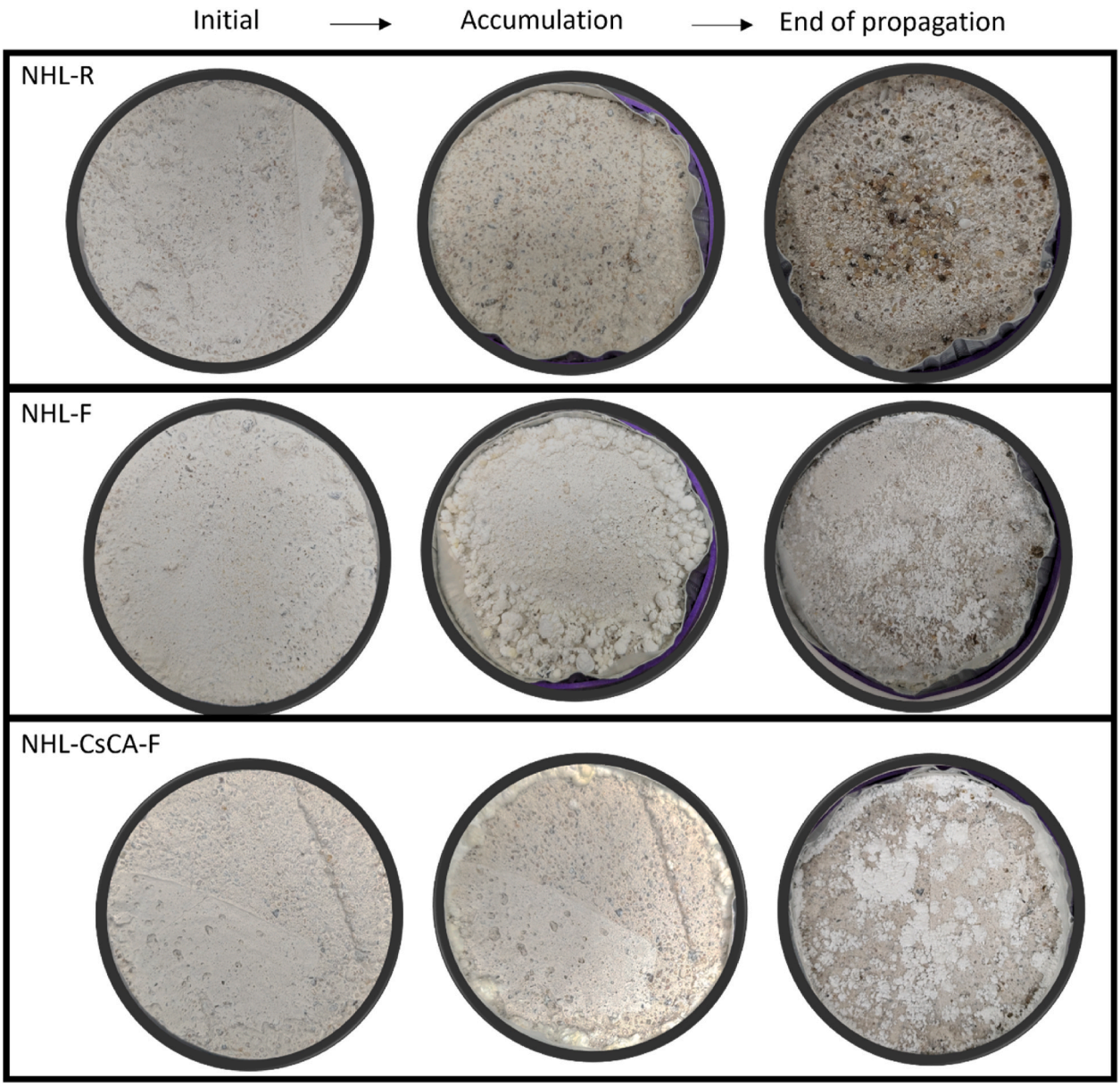

Fig. 5. Progression of damage in NHL-based mortars due to salt weathering test. The images are taken at the start of the test, at the end of the accumulation stage and the end of the propagation stage (four cycles). NHL-R shows material loss as sanding (loss of cohesion) of the fine aggregates. NHL-F and NHL-CsCA-F show a large amount of cauliflower-like salt efflorescence but no evidence of sanding of aggregates or a lack of cohesion.

the mortar matrix making it less susceptible to leaching.

The SEM images of the capsule (Fig. 4d and e) show that the capsules do not form any bond with the mortar matrix and is thus free to swell/shrink. No cracks were observed in the mortar matrix. This suggests, that capsules can swell and deswell when subjected to wet-dry cycles without imposing expansion stresses due to absence of any constraints.

3.2. Assessing mortar damage due to accelerated salt weathering test

The resistance of the mortars against salt crystallisation damage was assessed according to a procedure, adapted from the RILEM 271-ASC accelerated weathering test [39].

3.2.1. NHL-based mortar

Fig. 5 shows the progression of damage, as photographically assessed, on different NHL-based mortar specimens at the start of the test, at the end of the accumulation stage and at the end of the propagation stage (four cycles). At the end of the accumulation stage, all specimens show salt accumulation/efflorescence at the surface with no material damage (in accordance to the RILEM 271-ASC recommendations [39]). Among specimens containing the inhibitor, NHL-F shows considerably higher efflorescence than NHL-CsCA-F specimens. Damage starts developing during the propagation stage.

In NHL-R specimens (reference), the damage is observed after the first propagation cycle and progressively increases with each cycle (Appendix 1); at the end of the test severe material loss is observed (Fig. 5). The progressive damage is a result of the repeated deliquescence-recrystallisation cycles on salt crystals that have been shown to cause irreversible dilation in mortar [45] and an increased crystal size possibly exerting higher crystallisation pressure in the mortar pores [5]. The type of damage (i.e. sanding, according to Ref. [46]) as seen in these specimens is typically observed on plasters in the field [23], confirming the reliability of the test procedure to reproduce real case scenarios. At the end of the test, after brushing off the

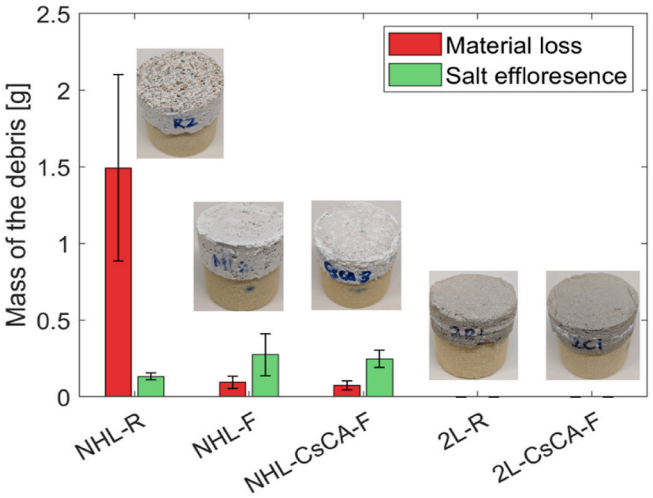

Fig. 6. The plot showing the material loss (red) and salt efflorescence (green) measured from each type of mortar specimen at the end of the accelerated test. The error bars indicate one standard deviation away from the mean. **Inset:** images of specimen surface corresponding to each mortar type obtained after brushing the debris.

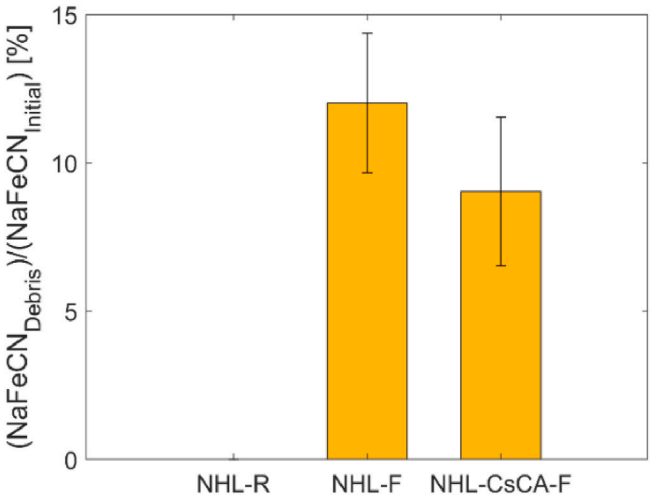

Fig. 8. NaFeCN measured by means of ICP-OES in the debris collected at the end of the test on NHL -based mortars. The results are expressed as a weight percentage of the initial NaFeCN amount present in each specimen. The error bars indicate one standard deviation away from the mean.

debris, a rough surface is observed due to loss of adhesion between the sand grains and the binder (Fig. 6). Specimens NHL-F and NHL-CsCA-F, containing NaFeCN mixed in and in encapsulated form respectively, show a large amount of salt efflorescence, which increases with each successive cycle (Appendix 1). At the end of the test, after brushing off the surface, only negligible surface damage is observed (Fig. 6).

In order to quantify the damage, the debris brushed off from the surface of the specimen at the end of the test was analysed as described in Section 2.5.3. Fig. 6 shows the total material loss and the amount of salt transported to the surface (as salt efflorescence) measured at the end of the test. NHL-R specimens exhibit severe material loss. Differently, mortars with mixed-in NaFeCN (NHL-F) and encapsulated inhibitor (NHL-CsCA-F) show almost 16 times lower material loss compared to NHL-R specimens and a higher salt efflorescence. When comparing mortars with encapsulated (NHL-CsCA-F) and mixed in NaFeCN (NHL-F), a similar amount of material loss and salt efflorescence is visible. These results confirm that the amount of NaFeCN released from the CsCA capsules is sufficient to prevent damage in mortar.

SEM observations have been performed on the cross-section of NHL-R and NHL-CsCA-F specimens to observe the change in NaCl crystal morphology due to the action of NaFeCN. The SEM images (Fig. 7) in the cross-section of both NHL-R and NHL-CsCA-F show that not all salt is transported outside the specimen and part of it crystallises within the mortar pores. In NHL-R (Fig. 7a), it can be observed that NaCl crystals have a cubic habit whereas, in NHL-CsCA-F specimens (Fig. 7b), NaFeCN leads to a change of crystal morphology, from cubic habit to dendritic growth, and a smaller crystal size as compared to NHL-R. These changes are in line with the previous studies demonstrating NaFeCN's ability to delay NaCl nucleation [17] and alter NaCl crystal morphology [16]. The former allows salt ions to remain longer in the solution without crystallising while the latter has shown to increase the advection of salts to the surface [20]. Consequently in specimens containing the inhibitor (NHL-F and NHL-CsCA-F), most of the salts crystallise on the surface of the mortar as efflorescence without exerting crystallisation pressure in the pores (See Figs. 5 and 6). This results in mitigating the damage

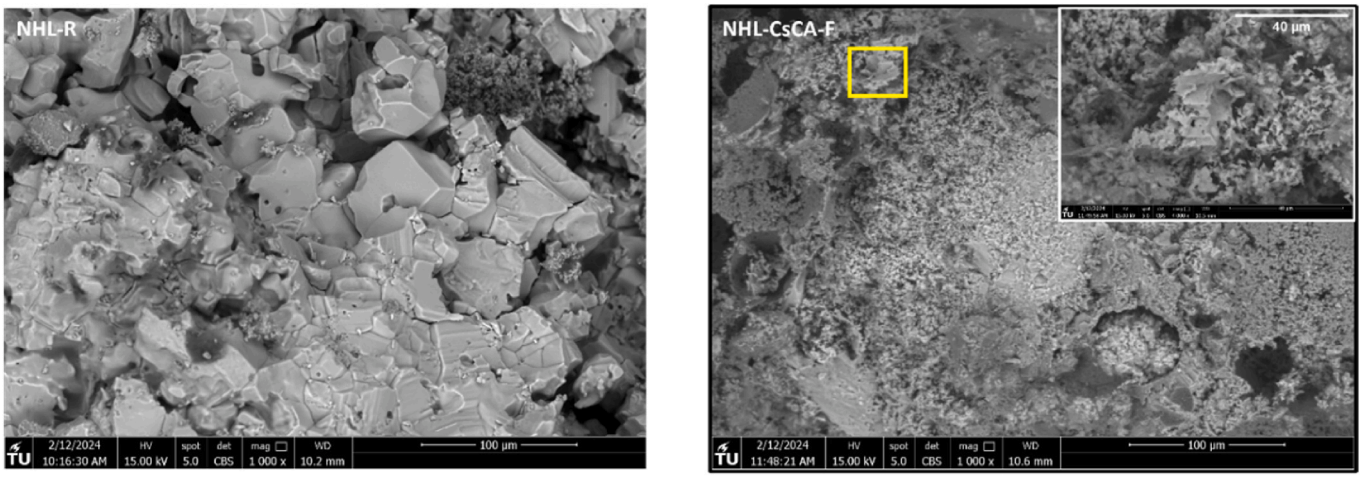

Fig. 7. SEM microscopic images of the cross-section of NHL-mortars at the end of the accelerated weathering test. Images are taken at about 1 mm from the evaporation surface **(a)** cubic NaCl crystals observed in the pores of the reference NHL mortar (NHL-R) which did not contain NaFeCN **(b)** Dendritic NaCl crystals in mortar NHL-CsCA-F. Note the small size of the crystal in comparison to (a) **Inset:** magnified image of the area marked in yellow showing the modified dendritic NaCl crystal habit.

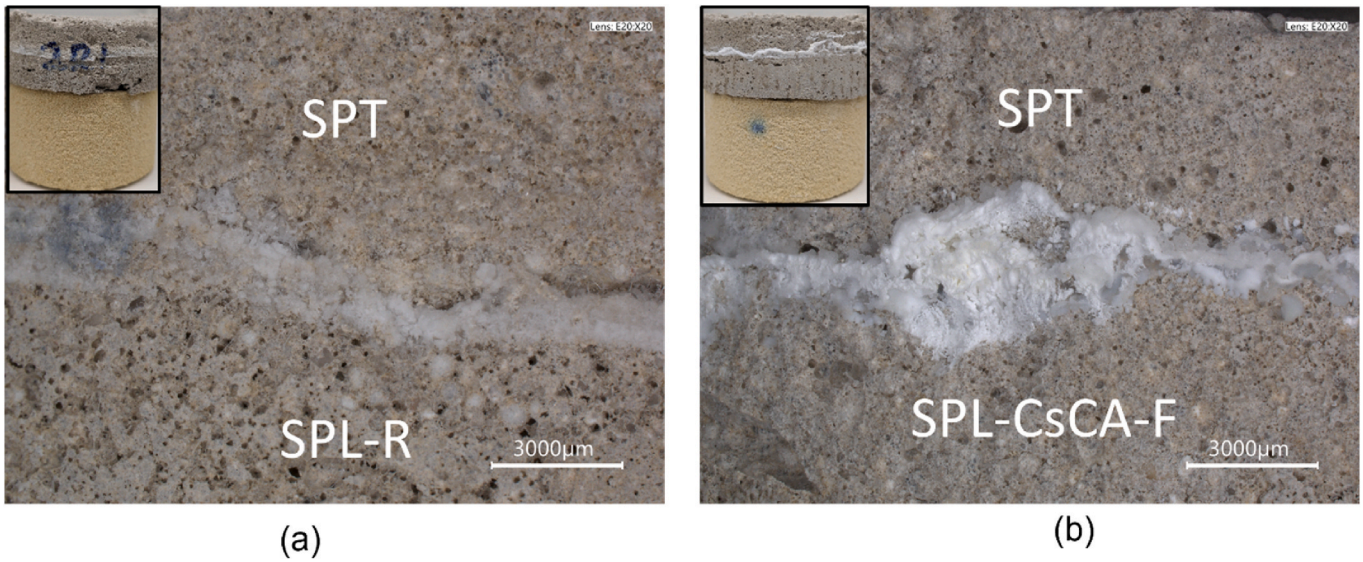

Fig. 9. Optical microscopy images showing NaCl accumulation in between the layers of the 2-layer plasters at the end of the accelerated weathering test **(a)** compact NaCl crystals in reference 2L-R mortar **(b)** dendritic NaCl crystals in 2L-CsCA-F mortar. **Inset:** high field of view images (digital camera) of both the specimens showing the extent of salt accumulation in between the layers.

induced by salt crystallisation. Moreover, the formation of smaller crystals (crystallites) within the pores as evident in Fig. 7b may have also contributed to lower pore-filling, consequently preventing salt damage in specimens containing NaFeCN, as suggested by Ref. [7].

When considering the amount of inhibitor leached out of the mortars, a higher efflorescence observed at the end of the accumulation stage in NHL-F specimens over NHL-CsCA-F specimens (Fig. 5) is a sign that most of the inhibitor from NHL-F may have already been transported to the surface during the accumulation stage itself. Debris analysis at the end of the test, shows that NHL-CsCA-F has a 30 % lower inhibitor leached out of the mortar in comparison to NHL-F, demonstrating that the CsCA capsules used in this study can slow down NaFeCN leaching (Fig. 8). As deduced from the previous study, slower release of the inhibitor from the capsules is attributed to chitosan's pH sensitive electrostatic interaction with ferrocyanide anions and chitosan's role in counteracting the swelling of alginate matrix [26]. This implies that encapsulation of the inhibitor can prolong its effectiveness over time and improve the service life of the inhibitor.

3.2.2. Two-layer cement-based plaster system

Both 2-layer cement-based plaster specimens (i.e. 2L-R and 2L-CsCA-F) do not show any visible surface damage at the end of the weathering test (Appendix 1). In both cases, independently from the presence of encapsulated inhibitor in the base layer, most of the salt crystallised in between the two mortar layers (Fig. 9). This behaviour show that the hydrophobic top layer (SPT) is able to stop liquid water and salt transport, as could be deduced based on the measured low WAC (Table 3).

Visual observations of the lateral sides of the specimens at the end of the test show the effect of NaFeCN on the crystal habit of NaCl crystallizing in 2L-R specimens (Fig. 9a) to a dendritic habit (Fig. 9b). As no damage was observed in both mortars with and without encapsulated inhibitor, no conclusion can be drawn on the positive effect of inhibitors in reducing crystallisation pressure in pores. No observed damage may be associated to a few reasons. The high mechanical strength of both the plaster layers (SPT and SPL) may have resisted the four damage propagation cycles (See Table 3). Second, the location of salts in between the two plaster layers, thus further away from the surface may have made it difficult for the small duration of RH cycles to dissolve and recrystallise salts in such depths. Thus, the currently employed crystallisation-deliquescence cycles may not be effective for such type of plaster system.

4. Conclusions and outlook

In this research, the effect of NaFeCN, inhibitor of NaCl crystallisation on the properties and durability with respect to salt crystallisation of hydraulic (NHL- and cement-based) mortars was investigated. The inhibitor was either mixed-in directly (in an aqueous solution) in the mortar or encapsulated in chitosan-calcium alginate capsules, which were added to the mortar during mixing. Various experimental techniques were used to assess the mechanical (compressive strength) and physical properties (porosity, pore size distribution, water absorption and drying behaviour) of the mortar. The durability of the mortar to NaCl-induced crystallisation damage was assessed using accelerated salt weathering test as per the RILEM- 271 recommendations. The results show that the addition of the inhibitor to the mortar, both in directly mixed-in and in encapsulated form, significantly reduce salt damage (material loss), without negatively affecting the properties of mortar. The reduction in salt damage in the presence of the inhibitor is a result of the delay in salt crystal nucleation and alteration of the crystal habit, thereby promoting harmless salt efflorescence over harmful subflorescence. Furthermore, encapsulation of the inhibitor in CsCA capsules was successful in reducing leaching of the inhibitor out of mortar, while still guaranteeing reduction in salt damage similar to mortars with mixed-in inhibitor. Reduction in leaching and a slower release of the inhibitor from the capsules is attributed to the presence of functional groups (amine) on chitosan in the CsCA capsules that prevent rapid release of the inhibitor [26]. These observations suggest that the slower release of the inhibitor from the capsules over a longer time is expected to prolong the service life of the inhibitor and improve the durability of mortars against salt damage.

For the future, some questions are left to be investigated. A long term monitoring programme with the application of the developed mortar prototype in a real-time field-study is planned along [23] in analysing long-term benefits of the encapsulated crystallisation inhibitor developed in this research. From the fundamental point of view, the supposed positive effect of NaFeCN on NaCl crystallisation pressure still needs to be experimentally assessed. Finally, the possibility of fine-tuning the composition of the capsules to adapt to the rate of inhibitor release based on the severity of the conditions (i.e. salt and moisture load) could be considered.

CRediT authorship contribution statement

Ameya Kamat: Writing – original draft, Visualization, Validation, Methodology, Investigation, Formal analysis, Conceptualization. **Erik Schlangen:** Writing – review & editing, Supervision, Project administration, Methodology, Funding acquisition, Conceptualization. **Barbara Lubelli:** Writing – review & editing, Supervision, Project administration, Funding acquisition, Conceptualization.

Declaration of competing interest

The authors declare that they have no known competing financial interests or personal relationships that could have appeared to influence the work reported in this paper.

Data availability

Data will be made available on request.

Acknowledgments

The research is funded by NWO (Dutch research council) under the project 'Mortars with mixed-in inhibitors for mitigating salt damage-MORISAL' (Grant no. 17636). The authors thank Dr. Timo Nijland (TNO) for his help with thin-section preparation and optical microscopy; Mr. Vincent Crevals and Mr. Sebastian Godts from KIK-IRPA, Belgium for their help with MIP. The authors are also grateful to Mr. John van den Berg and Mr. Arjan Thijssen for their help with ICP-OES measurements and SEM observation respectively.

Appendix 1. Damage progression after each propagation cycle

I=Initial before testing, A = Accumulation, P1=Propagation cycle 1, P2=Propagation cycle 2, P3=Propagation cycle 3, P4=Propagation cycle 4, E = End of the test after brushing the debris.

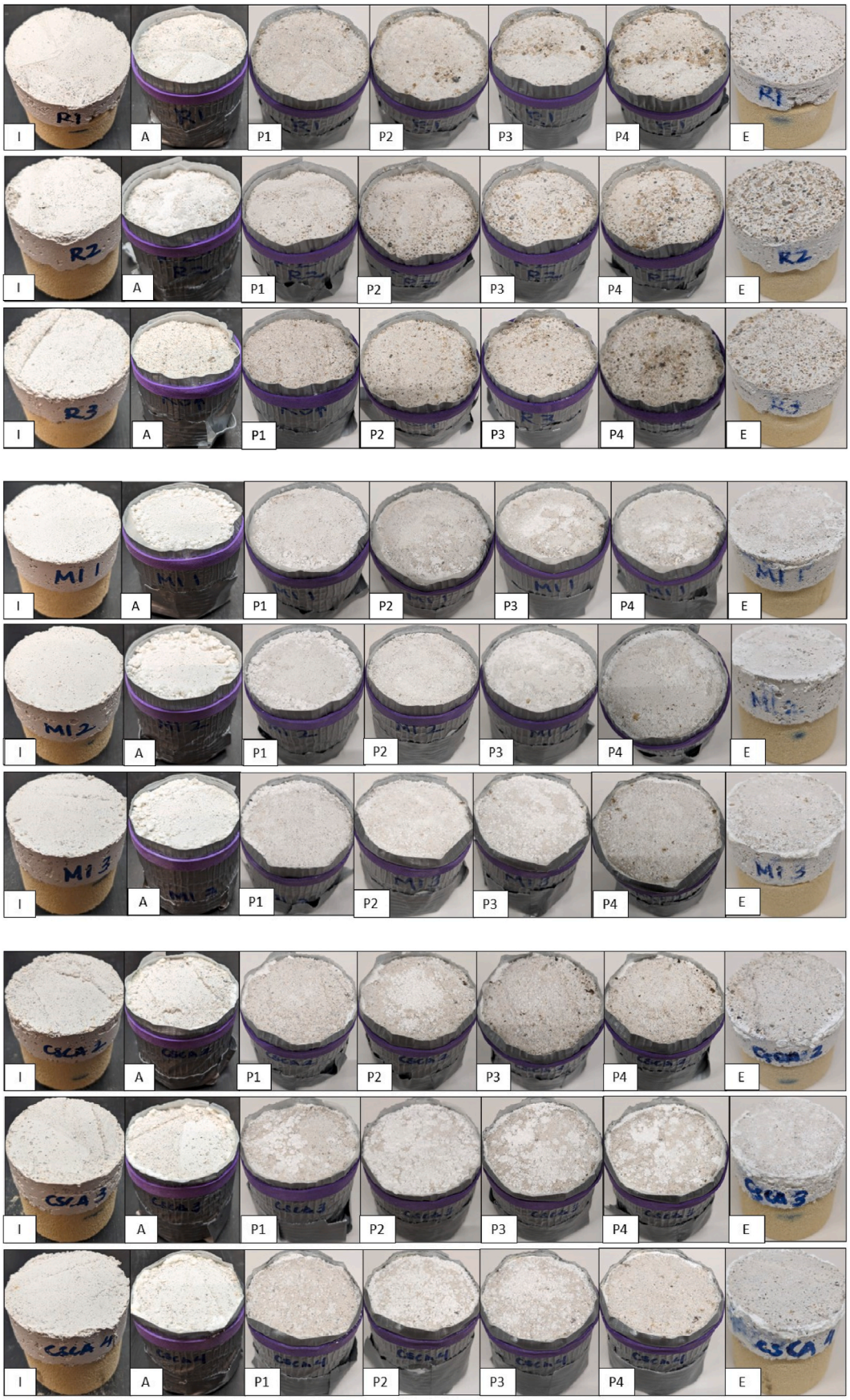
I
A
P1
P2
P3
P4
E
NHL-R (1)
NHL-R (2)
NHL-R (3)
NHL-F (1)
NHL-F (2)
NHL-F (3)
NHL-CsCA-F (1)
NHL-CsCA-F (2)
NHL-CsCA-F (3)

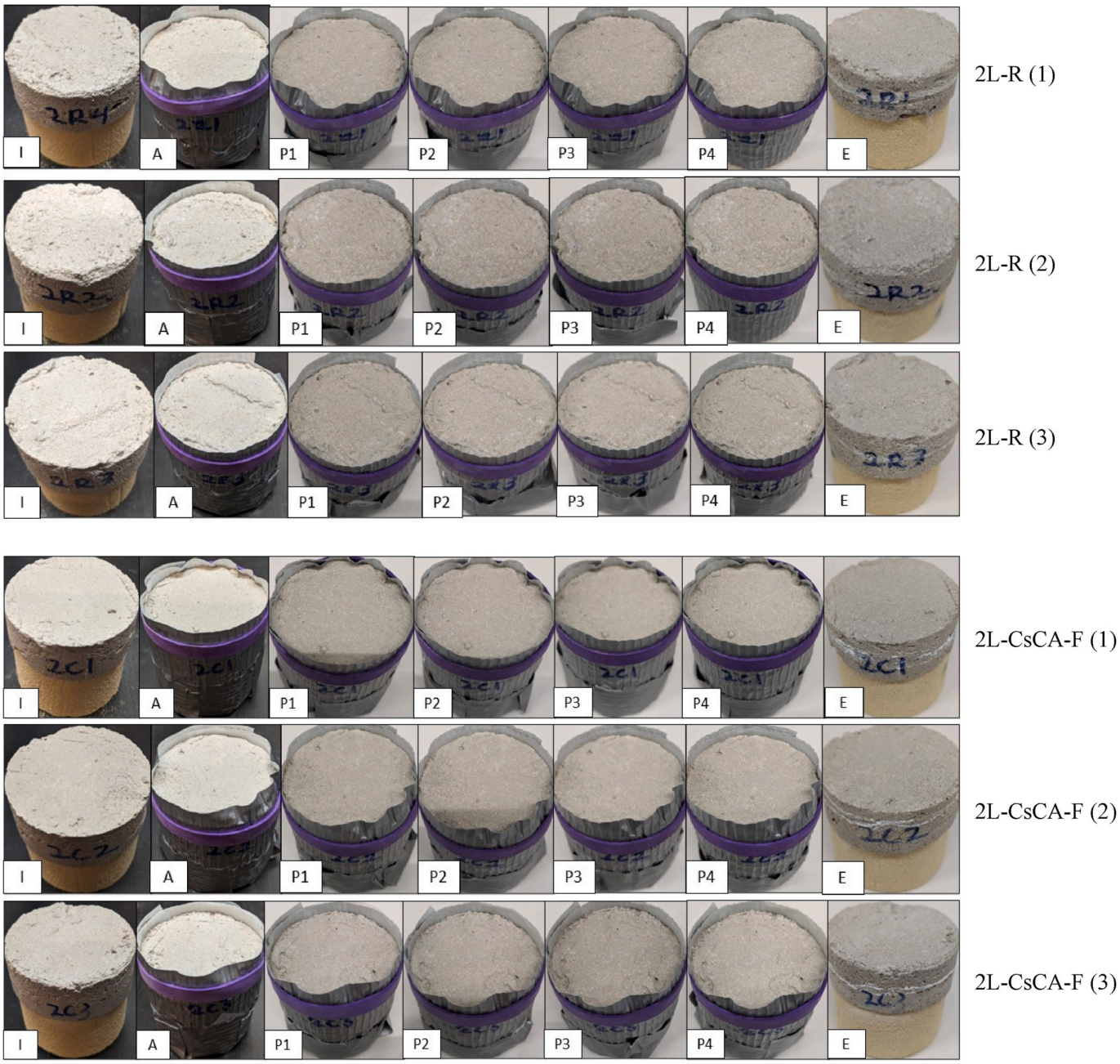

References

[1] A. Goudie, H. Viles, Salt Weathering Hazards, John Wiley & Sons Ltd, Chichester, 1997.

[2] A.E. Charola, Salts in the deterioration of porous materials : an overview, J. Am. Inst. Conserv. 39 (2000) 327–343, https://doi.org/10.1179/019713600806113176.

[3] M. Steiger, Crystal growth in porous materials - I: the crystallization pressure of large crystals, J. Cryst. Growth 282 (2005) 455–469, https://doi.org/10.1016/j.jcrysgro.2005.05.007.

[4] G.W. Scherer, Stress from crystallization of salt, Cement Concr. Res. 34 (2004) 1613–1624, https://doi.org/10.1016/j.cemconres.2003.12.034.

[5] J. Desarnaud, N. Shahidzadeh-Bonn, Salt crystal purification by deliquescence/crystallization cycling, EPL (Europhysics Lett. 95 (2011) 48002, https://doi.org/10.1209/0295-5075/95/48002.

[6] B. Lubelli, R.P.J. van Hees, C.J.W.P. Groot, The effect of environmental conditions on sodium chloride damage: a step in the development of an effective weathering test, Stud. Conserv. 51 (2006) 41–56, https://doi.org/10.1179/sic.2006.51.1.41.

[7] S.J.C. Granneman, B. Lubelli, R.P.J. van Hees, Effect of mixed in crystallization modifiers on the resistance of lime mortar against NaCl and Na2SO4 crystallization, Construct. Build. Mater. 194 (2019) 62–70, https://doi.org/10.1016/j.conbuildmat.2018.11.006.

[8] C. Rodriguez-Navarro, L.G. Benning, Control of crystal nucleation and growth by additives, Elements 9 (2013) 203–209, https://doi.org/10.2113/gselements.9.3.203.

[9] E. Ruiz-Agudo, C. Rodriguez-Navarro, E. Sebastián-Pardo, Sodium sulfate crystallization in the presence of phosphonates: implications in ornamental stone conservation, Cryst. Growth Des. 6 (2006) 1575–1583, https://doi.org/10.1021/cg050503m.

[10] M.M. Saleh, S.S. Darwish, M. Elzoghby, The effectiveness of some crystallization inhibitors in preventing salt damage to limestone, J. Cryst. Growth 585 (2022) 126606, https://doi.org/10.1016/j.jcrysgro.2022.126606.

[11] E.R. Townsend, F. Swennenhuis, W.J.P. Van Enckevort, J.A.M. Meijer, E. Vlieg, Creeping: an efficient way to determine the anticaking ability of additives for sodium chloride, CrystEngComm 18 (2016) 6176–6183, https://doi.org/10.1039/c6ce01376g.
[12] A.A.C. Bode, V. Vonk, F.J. Van Den Bruele, D.J. Kok, A.M. Kerkenaar, M. F. Mantilla, S. Jiang, J.A.M. Meijer, W.J.P. Van Enckevort, E. Vlieg, Anticaking activity of ferrocyanide on sodium chloride explained by charge mismatch, Cryst. Growth Des. 12 (2012) 1919–1924, https://doi.org/10.1021/cg201661y.
[13] S.J.C. Granneman, B. Lubelli, R.P.J. van Hees, Mitigating salt damage in building materials by the use of crystallization modifiers – a review and outlook, J. Cult. Herit. 40 (2019) 183–194, https://doi.org/10.1016/j.culher.2019.05.004.
[14] M.A.R. Blijlevens, E.R. Townsend, P. Tinnemans, W.J.P. van Enckevort, E. Vlieg, Effect of the anticaking agent FeCN on the creeping properties of alkali halide crystals, Cryst. Growth Des. 22 (2022) 6575–6581, https://doi.org/10.1021/acs.cgd.2c00786.
[15] A. Glasner, M. Zidon, The crystallization of NaCl in the presence of [Fe(CN)6]4- ions, J. Cryst. Growth 21 (1974) 294–304, https://doi.org/10.1016/0022-0248(74)90018-9.
[16] C. Rodriguez-Navarro, L. Linares-Fernandez, E. Doehne, E. Sebastian, Effects of ferrocyanide ions on NaCl crystallization in porous stone, J. Cryst. Growth 243 (2002) 503–516, https://doi.org/10.1016/S0022-0248(02)01499-9.
[17] C. Selwitz, E. Doehne, The evaluation of crystallization modifiers for controlling salt damage to limestone, J. Cult. Herit. 3 (2002) 205–216, https://doi.org/10.1016/S1296-2074(02)01182-2.
[18] B. Lubelli, R.P.J. van Hees, Effectiveness of crystallization inhibitors in preventing salt damage in building materials, J. Cult. Herit. 8 (2007) 223–234, https://doi.org/10.1016/j.culher.2007.06.001.
[19] T. Rivas, J. Feijoo, I. de Rosario, J. Taboada, Use of ferrocyanides on granite desalination by immersion and poultice-based methods, Int. J. Architect. Herit. 11 (2017) 588–606, https://doi.org/10.1080/15583058.2016.1277282.
[20] S. Gupta, K. Terheiden, L. Pel, A. Sawdy, Influence of ferrocyanide inhibitors on the transport and crystallization processes of sodium chloride in porous building materials, Cryst. Growth Des. 12 (2012) 3888–3898, https://doi.org/10.1021/cg3002288.
[21] B. Lubelli, T.G. Nijland, R.P.J. Van Hees, A. Hacquebord, Effect of mixed in crystallization inhibitor on resistance of lime-cement mortar against NaCl crystallization, Construct. Build. Mater. 24 (2010) 2466–2472, https://doi.org/10.1016/j.conbuildmat.2010.06.010.
[22] J. Feijoo, D. Ergenç, R. Fort, M.A. de Buergo, Addition of ferrocyanide-based compounds to repairing joint lime mortars as a protective method for porous building materials against sodium chloride damage, Mater. Struct. 54 (2021) 14, https://doi.org/10.1617/s11527-020-01596-4.
[23] B. Lubelli, E. des Bouvrie, T.G. Nijland, A. Kamat, Plasters with mixed-in crystallization inhibitors: results of a 4-year monitoring of on-site application, J. Cult. Herit. 59 (2023) 10–22, https://doi.org/10.1016/j.culher.2022.10.016.
[24] A. Kamat, B. Lubelli, E. Schlangen, Effect of a mixed-in crystallization inhibitor on the properties of hydraulic mortars, AIMS Mater. Sci. 9 (2022) 628–641, https://doi.org/10.3934/matersci.2022038.
[25] A. Kamat, B. Lubelli, E. Schlangen, Leaching behaviour of a crystallisation inhibitor in mortars, J. Build. Eng. 79 (2023) 107933, https://doi.org/10.1016/j.jobe.2023.107933.
[26] A. Kamat, D. Palin, B. Lubelli, E. Schlangen, Capsule controlled release of crystallisation inhibitors in mortars, Mater. Des. 244 (2024) 113156, https://doi.org/10.1016/j.matdes.2024.113156.
[27] A. Kamat, D. Palin, B. Lubelli, E. Schlangen, Tunable chitosan-alginate capsules for a controlled release of crystallisation inhibitors in mortars, MATEC Web Conf. 378 (2023) 02011, https://doi.org/10.1051/matecconf/202337802011.
[28] J.Y. Wang, H. Soens, W. Verstraete, N. De Belie, Self-healing concrete by use of microencapsulated bacterial spores, Cement Concr. Res. 56 (2014) 139–152, https://doi.org/10.1016/j.cemconres.2013.11.009.
[29] C. Schröfl, K.A. Erk, W. Siriwatwechakul, M. Wyrzykowski, D. Snoeck, Recent progress in superabsorbent polymers for concrete, Cement Concr. Res. 151 (2022) 106648, https://doi.org/10.1016/j.cemconres.2021.106648.
[30] NEN-EN 196-1, Methods of Testing Cement - Part 1, Determination of strength, 2015.
[31] C. Nunes, A. Maria Aguilar Sanchez, S. Godts, D. Gulotta, I. Ioannou, B. Lubelli, B. Menendez, N. Shahidzadeh, Z. Slížková, M. Theodoridou, Experimental research on salt contamination procedures and methods for assessment of the salt distribution, Construct. Build. Mater. 298 (2021) 123862, https://doi.org/10.1016/j.conbuildmat.2021.123862.
[32] E.-S. Chan, B.-B. Lee, P. Ravindra, D. Poncelet, Prediction models for shape and size of ca-alginate macrobeads produced through extrusion–dripping method, J. Colloid Interface Sci. 338 (2009) 63–72, https://doi.org/10.1016/j.jcis.2009.05.027.
[33] W.R. Gombotz, S.F. Wee, Protein release from alginate matrices, Adv. Drug Deliv. Rev. 31 (1998) 267–285, https://doi.org/10.1016/S0169-409X(97)00124-5.
[34] NEN-EN 459-2, Building Lime-Part 2: Test Methods, 2008.
[35] NEN-EN 1015-11, Methods of Test for Mortar for Masnory-Part 11: Determination of Flexural and Conpressive Strength of Hardened Mortar, 2019.
[36] NEN-EN 1015-3, Methods of Test for Mortar for Masonry - Part 3: Determination of Consistence of Fresh Mortar (By Flow Table), 1999.
[37] NEN-EN-1925, Natural Stone Test Methods- Determination of Water Absorption Coefficient by Capillarity, 1999.
[38] T.G. Nijland, J.A. Larbi, Microscopic examination of deteriorated concrete, in: Non-Destructive Eval. Reinf. Concr. Struct., Elsevier, 2010, pp. 137–179, https://doi.org/10.1533/9781845699536.2.137.
[39] B. Lubelli, I. Rörig-Daalgard, A.M. Aguilar, M. Aškrabić, K. Beck, C. Bläuer, V. Cnudde, A.M. D'Altri, H. Derluyn, J. Desarnaud, T. Diaz Gonçalves, R. Flatt, E. Franzoni, S. Godts, D. Gulotta, R. van Hees, I. Ioannou, A. Kamat, T. De Kock, B. Menendez, S. de Miranda, C. Nunes, E. Sassoni, N. Shahidzadeh, H. Siedel, Z. Slížková, M. Stefanidou, M. Theodoridou, R. Veiga, V. Vergès-Belmin, Recommendation of RILEM TC 271-ASC: new accelerated test procedure for the assessment of resistance of natural stone and fired-clay brick units against salt crystallization, Mater. Struct. 56 (2023) 101, https://doi.org/10.1617/s11527-023-02158-0.
[40] B. Lubelli, A.M. Aguilar, K. Beck, T. De Kock, J. Desarnaud, E. Franzoni, D. Gulotta, I. Ioannou, A. Kamat, B. Menendez, I. Rörig-Dalgaard, E. Sassoni, A new accelerated salt weathering test by RILEM TC 271-ASC: preliminary round robin validation, Mater. Struct. 55 (2022) 238, https://doi.org/10.1617/s11527-022-02067-8.
[41] M. George, T.E. Abraham, Polyionic hydrocolloids for the intestinal delivery of protein drugs: alginate and chitosan - a review, J. Contr. Release 114 (2006) 1–14, https://doi.org/10.1016/j.jconrel.2006.04.017.
[42] A. Mignon, G.-J. Graulus, D. Snoeck, J. Martins, N. De Belie, P. Dubruel, S. Van Vlierberghe, pH-sensitive superabsorbent polymers: a potential candidate material for self-healing concrete, J. Mater. Sci. 50 (2015) 970–979, https://doi.org/10.1007/s10853-014-8657-6.
[43] J. Liu, N. Farzadnia, C. Shi, Microstructural and micromechanical characteristics of ultra-high performance concrete with superabsorbent polymer (SAP), Cement Concr. Res. 149 (2021) 106560, https://doi.org/10.1016/j.cemconres.2021.106560.
[44] Y. Li, H. Luo, B. Zhang, X. Wei, F. Wang, W. Wang, P. Liu, J. Zhu, Internal curing of natural hydraulic lime with superabsorbent polymers, Mater. Today Commun. 34 (2023) 105064, https://doi.org/10.1016/j.mtcomm.2022.105064.
[45] B. Lubelli, R.P.J. Van Hees, H.P. Huinink, C.J.W.P. Groot, Irreversible dilation of NaCl contaminated lime-cement mortar due to crystallization cycles, Cement Concr. Res. 36 (2006) 678–687, https://doi.org/10.1016/j.cemconres.2005.10.008.
[46] Monument diagnosis and conservation system (n.d.), https://mdcs.monumentenkennis.nl/damageatlas/269/category#overview. (Accessed 13 March 2024).